**Title:** Differential scanning calorimetric study of solidification behavior of monoglycerides to investigate cold-flow properties of biodiesel

**Running title:** Thermodynamics of binary monoglycerides

**Authors:** Latifa Seniorita[1], Eiji Minami[1], Yoshiteru Yazawa[2], Hitoshi Hayashi[2], Shiro Saka[1]

**Affiliations:**

1. Graduate School of Energy Science, Kyoto University, Japan

2. Material Engineering Division No.2, Toyota Motor Corporation, Japan

**Corresponding author:** Eiji Minami

**Address:** Graduate School of Energy Science, Kyoto University, Yoshida-honmachi, Sakyo-ku, Kyoto 606-8501, Japan

**Tel/Fax:** +81 (0)75 753 5713

**E-mail:** minami@energy.kyoto-u.ac.jp

**Abstract:**

Monoglycerides (MGs) are impurities present in biodiesel as a result of incomplete reactions. MGs often solidify in biodiesel even at room temperature because of their high melting points. This worsens the cold-flow properties such as the cloud point and pour point. We hypothesized that several types of MGs solidify simultaneously; therefore we performed differential scanning calorimetry of binary mixtures of MGs to elucidate their interactions during solidification. Three thermodynamic formulas were then applied to the experimental results: 1) non-solid-solution, 2) solid-solution, and 3) compound formation models. Binary mixtures of MGs showed complicated liquidus curves with multiple upward convex shapes, with which only the compound formation model fitted well. This model was applied to multi-component mixtures that consisted of MGs and fatty acid methyl esters as surrogate biodiesel fuels. We confirmed that the model still worked well. The results show that the compound formation model has good potential for predicting the cold-flow properties of biodiesel.

**Keywords:** Biodiesel, Polymorphism, Thermal analysis

## Introduction

Biodiesel is a mixture of fatty acid methyl esters (FAMEs), which are produced by transesterification of plant oils, and is used as a fossil diesel substitute. It is renewable and has a low sulfur content but poor cold-flow properties (CFPs) compared with those of fossil diesel. The CFPs such as the cloud point and pour point determine the low-temperature fluidity of a liquid fuel. Prediction of biodiesel CFPs is therefore important for minimizing the risk of fuel clogging.

Many models for predicting biodiesel CFPs have been reported (Imahara et al., 2006; Lopes et al., 2008; Sarin et al., 2009; Coutinho et al., 2010; Dunn, 2010). Saturated FAMEs such as methyl palmitate greatly affect the CFPs because of their high melting points (Dunn and Bagby, 1995; Knothe, 2005). Sarin et al. (2009) established regression formulas for predicting the cloud point and pour point as a linear function of methyl palmitate content for biodiesel fuels from palm (*Elaeis guineensis*), jatropha (*Jatropha curcas*), and pongamia (*Pongamia pinnata*) oils. Such empirical models are simple and easy to use, but not applicable to biodiesel fuels from other feedstocks because the fatty acid compositions are different. Some research groups have investigated thermodynamic models that are applicable to any biodiesel (Imahara et al., 2006; Lopes et al., 2008; Coutinho et al., 2010). Imahara et al. (2006) calculated the solid–liquid equilibria of FAME mixtures, with the assumption of ideal liquid solutions, and found that the theoretical liquidus temperatures were in good

agreement with the experimental cloud points. The liquidus temperature is defined as the temperature above which a given mixture is completely in the liquid phase. A solid phase can form when the mixture is cooled below the liquidus temperature, therefore it is an important index for predicting CFPs.

The thermodynamic models (Imahara et al., 2006; Lopes et al., 2008; Coutinho et al., 2010) were based on the theory of solid-liquid equilibrium, where the fugacity of each component is equal in solid and liquid phases. This theory expresses the relationship between the liquidus temperature and properties of the mixture, such as chemical composition, melting point and enthalpy of fusion of each component. The liquidus temperature is thus predicted from the properties of the mixture. The theory is well described in a textbook of chemical physics (Smith et al., 2005).

The presence of minor components also considerably affects the CFPs. Monoglycerides (MGs), which are intermediate compounds produced during transesterification, are typical minor components in biodiesel, and the European standard restricts the total amount of MGs to below 0.8 wt% (Committee for Standardization Automatic Fuels, 2008). MGs occasionally solidify even at around room temperature because their melting points are high (Tang et al., 2008; Chupka et al., 2011; Chupka et al., 2014). MGs have various crystalline structures, namely α, β′, and β types, and each has a different melting point in the following order, $\alpha < \beta' < \beta$ (Fischer et al., 1920; Malkin and Shurbagy,

58 1936). In general, α-type crystals form first when a liquid MG is cooled until the phase
59 transition occurs. The α crystals are converted irreversibly to the β′ type and then to the β
60 type after specific transition times (Maruyama et al., 1973). The potential presence of several
61 polymorphs makes the solidification behavior of MGs complicated. Chupka et al. studied the
62 effects of MGs on biodiesel CFPs and highlighted the importance of MG polymorphism
63 (Chupka et al., 2011; Chupka et al., 2014).

64 Our research group previously developed a thermodynamic model for calculating
65 the solid–liquid equilibria of surrogate biodiesel fuels containing MGs (Yoshidomi et al.,
66 2017; Sugami et al., 2017). We found that a binary mixture of a MG and a FAME behaves as
67 a non-ideal liquid solution because of the large difference between the chemical structures of
68 the components, and the non-ideality is well described by a modified version of the universal
69 quasi-chemical functional-group activity coefficients (UNIFAC) model, known as the
70 UNIFAC (Dortmund) model (Gmehling et al., 1993). When the mixture contains only one
71 type of MG, the predicted values are in excellent agreement with the experimental results.
72 However, deviations arise when the mixture includes two different MGs (Yoshidomi et al.,
73 2017; Sugami et al., 2017). We hypothesized that this discrepancy is caused by
74 co-crystallization (solid solution) of the different MGs, because our previous model assumed
75 that the solid phase consists of a single component. Lutton and Jackson (1967) and
76 Maruyama et al. (1978) have reported the formation of such solid solutions of different MGs

77 under certain conditions.

78 The aim of the current study was to use differential scanning calorimetry (DSC) to
79 investigate the interactions between MGs and to develop an appropriate thermodynamic
80 model for describing the solidification behaviors of MGs. The model obtained was then
81 applied to multi-component mixtures, which contained two types of MGs in FAMEs and
82 served as surrogate biodiesel fuels. The results of this study will help to establish a
83 prediction model for real biodiesel, which contains several types of MGs.

84

85 **Experimental Procedures**

86 Materials

87 The MG samples used were 1-monolaurin (MG12:0, purity 99%, Tokyo Chemical
88 Industry, Tokyo, Japan), 1-monopalmitin (MG16:0, 99%, Olbracht Serdary Research
89 Laboratories (OSRL), Toronto, Canada), and 1-monostearin (MG18:0, 99%, OSRL). The
90 FAME samples were methyl laurate (FAME12:0, 99%), methyl palmitate (FAME16:0, 99.5%),
91 and methyl oleate (FAME18:1, 99%), which were all purchased from Sigma-Aldrich Japan,
92 Tokyo. Test samples for DSC were prepared by blending these chemicals in various ratios,
93 without purification.

94

95

96 Analytical methods

97 For DSC analyses, samples (about 10 mg) were placed in non-hermetic
98 aluminum-based pans under a dry nitrogen flow. Indium and zinc were used for temperature
99 calibration and α-alumina was used as a reference material. We determined the liquidus
100 temperature for each sample from the obtained DSC profile. Because MGs are polymorphic,
101 we used two different methods for examining α- and β-type crystals.

102 For α-type crystals, each sample was heated until fully melted and cooled until the
103 first exothermic peak was detected; the solid phase formed at this time is thought to consist
104 of α-type crystals (Maruyama et al., 1973; Yoshidomi et al., 2017). The sample was then
105 reheated immediately at a heating rate of 3 °C/min and the DSC profile was recorded. This
106 rapid heating prevents the crystal transition to the β′ or β type during analysis. For β-type
107 crystals, each solidified sample was held in a thermostatic chamber at 50 °C for four weeks to
108 ensure the transition to the β type, which is the most stable structure. The reported times for
109 transition to the β type are about 0.1, 100, and 230 h at 50 °C for MG12:0, MG16:0, and
110 MG18:0, respectively (Maruyama et al., 1971); four weeks (672 h) is therefore considered to
111 be sufficient. After removal from the chamber, the sample was exposed at room temperature
112 for a few minutes, and then DSC was performed at a heating rate of 1 °C/min.

113 For each pure MG, the melting point was estimated from the onset temperature of
114 the endothermic peak in the DSC profile. In the case of a binary or multi-component mixture,

115 the highest endothermic peak maximum temperature was defined as the experimental liquidus
116 temperature, as in previous studies (Maruyama et al., 1971; Knothe and Dunn, 2009;
117 Yoshidomi et al., 2017). Note that this is a rough estimate because the absolute liquidus
118 temperature is generally difficult to determine, especially for multi-component systems.
119
120 Thermodynamic models
121 Three thermodynamic models were used to calculate the liquidus temperatures. The
122 first two models were based on the solid–liquid equilibrium and the third was derived from
123 the reaction equilibrium. The calculations were conducted using programs coded with
124 Microsoft Visual Basic for Applications on Excel.
125
126 *Solid–liquid equilibrium*
127 At solid–liquid equilibrium, the fugacity of each component *i* in a given system is
128 the same in the solid (S) and liquid (L) phases; this relationship is expressed by the following
129 equation:
130 $$\gamma_i^{\mathrm{L}} x_i f_i^{\mathrm{L}} = \gamma_i^{\mathrm{S}} z_i f_i^{\mathrm{S}} \quad (1)$$
131 where $x_i$ and $z_i$ are the mole fractions of component *i* in the liquid and solid phases,
132 respectively, and $\gamma_i$ is the activity coefficient of component *i* in the mixture. The fugacity
133 ratio $f_i^{\mathrm{S}}/f_i^{\mathrm{L}}$ of the pure component *i* can be approximately expressed using the melting point

($T_{m,i}$) and enthalpy of fusion ($\Delta H_{m,i}$) of the pure component $i$ as follows (Smith et al, 2005):

$$\frac{\gamma_i^{L} x_i}{\gamma_i^{S} z_i} = \frac{f_i^{S}}{f_i^{L}} = \exp\frac{\Delta H_{m,i}}{RT_{m,i}}\left(\frac{T-T_{m,i}}{T}\right) \quad (2)$$

Two assumptions were made when using equation (2) to calculate the liquidus temperature $T$ of a given mixture. The first, which was used in the non-solid-solution model, is that the solid phase consists of a single component ($z_i$ = 1, therefore $\gamma_i^{S}$ = 1). This means that different MGs are immiscible in the solid phase. For a binary mixture, the relationship between the mole fraction and liquidus temperature is given by

$$\gamma_1^{L} x_1 = \exp\frac{\Delta H_{m,1}}{RT_{m,1}}\left(\frac{T-T_{m,1}}{T}\right) \text{ or } \gamma_2^{L} x_2 = \exp\frac{\Delta H_{m,2}}{RT_{m,2}}\left(\frac{T-T_{m,2}}{T}\right) \quad (3)$$

The second assumption, which was used in the solid-solution model, is that different MGs can form a continuous solid solution ($z_i \neq 1$) but the solution is ideal ($\gamma_i^{S}$ = 1). In this case, the liquidus temperature can be determined from the following equation:

$$\left[\gamma_1^{L} x_1 / \exp\frac{\Delta H_{m,1}}{RT_{m,1}}\left(\frac{T-T_{m,1}}{T}\right)\right] + \left[\gamma_2^{L} x_2 / \exp\frac{\Delta H_{m,2}}{RT_{m,2}}\left(\frac{T-T_{m,2}}{T}\right)\right] = 1 \quad (4)$$

This is derived from equation (2) and $z_1 + z_2 = 1$. For both models, the activity coefficients in the liquid phase, $\gamma_i^{L}$, were calculated using the UNIFAC (Dortmund) model (Gmehling et al, 1993), as in our previous studies (Yoshidomi et al, 2017; Sugami et al, 2017).

*Reaction equilibrium*

This model assumes that the solidification of MGs is similar to a chemical reaction. When $\nu_1$ moles of $C_1$ and $\nu_2$ moles of $C_2$ in a liquid phase produce a solid compound $C_3$, the

153 reaction is expressed as follows:

154 $$v_1 C_1(\text{liquid}) + v_2 C_2(\text{liquid}) \leftrightarrow C_3(\text{solid}) \quad (5)$$

155 The reaction equilibrium constant $K_a$ is described by

156 $$K_a = \frac{(\gamma_1{}^{\text{L}} x_1)^{v_1}(\gamma_2{}^{\text{L}} x_2)^{v_2}}{(z_3)^1} = (\gamma_1 x_1)^{v_1}(\gamma_2 x_2)^{v_2} \quad (6)$$

157 where $\gamma_i{}^{\text{L}}$ and $x_i$ are the activity coefficient and mole fraction of component $C_i$ in the liquid

158 phase, respectively. The term $z_3$ is the mole fraction of compound $C_3$ in the solid phase, but

159 because no other solid is present in the system, it can be assumed to be unity. However, there

160 is another expression for the equilibrium constant $K_a$, which is derived from the Gibbs–

161 Helmholtz equation (Tumakaka et al., 2007):

162 $$K_a = K_{\text{ref}} \times \exp\frac{\Delta H_{\text{ref}}}{R T_{\text{ref}}}\left(\frac{T - T_{\text{ref}}}{T}\right) \quad (7)$$

163 where $K_{\text{ref}}$ and $\Delta H_{\text{ref}}$ are the equilibrium constant and enthalpy of reaction, respectively, at an

164 arbitrarily chosen reference temperature $T_{\text{ref}}$. By combining equations (6) and (7), we can

165 determine the liquidus temperature $T$. This model was built according to the method reported

166 by Tumakaka et al. (2007) and is referred to as the compound formation model. The detailed

167 calculation procedure will be described in the following section. It should be noted that $v_1$

168 and $v_2$ can be used as fitting parameters in this model. The $\gamma_i{}^{\text{L}}$ terms were estimated by using

169 the UNIFAC (Dortmund) model.

170

171

## Results and Discussion

### Pure component properties

All three thermodynamic models involve pure component properties: the melting point $T_m$ and enthalpy of fusion $\Delta H_m$. We therefore used DSC to determine these properties for each pure MG and all crystalline forms; the results are shown in Table 1. We measured three times for each component and chose the middle value. The error ranges were -0.7 ~ +1.2 °C for melting point and -14 ~ +10% for enthalpy. The relatively large error for enthalpy might be because of the measurement error of the sample weight (only 10 mg). However, this error did not critically affect the calculation results.

The values obtained were consistent with those previously reported (Lutton, 1971; Maruyama et al., 1971; Yoshidomi et al., 2017), therefore we used them for performing calculations with equations (3), (4), and (7). The numbers of functional groups in each MG are also shown in Table 1; they were used to estimate the activity coefficients $\gamma_i^L$ with the UNIFAC (Dortmund) model.

### Binary MG behaviors

Various binary mixtures were analyzed by DSC. Figure 1 shows DSC profiles of the mixture of MG16:0 and MG18:0 for α- and β-type crystals. The endothermic peaks on DSC profiles indicate the phase transition from solid to liquid because melting is an endothermic

191 reaction. The liquidus temperature was determined from the endothermic peak maximum
192 temperature for each mixture. Because β-type MG crystal has a higher melting point than that
193 of α-type, the liquidus temperatures of β-type crystal were sifted to higher temperatures than
194 those of α-type.

195 The liquidus temperatures of α- and β-type crystals are shown by solid circles in
196 Figures 2 and 3, respectively, for various binary mixtures of MGs. Each measurement for
197 α-type crystal was conducted twice and the first result was chosen; the absolute deviation
198 between the first and second was within 1.3 °C for any mixtures studied. The β-type crystal
199 was measured once because the sample preparation took four weeks to ensure the transition
200 into β-type.

201 We can obtain the liquidus curves of the binary MGs by connecting these points.
202 The experimental liquidus curves have complex shapes, although we previously reported
203 (Yoshidomi et al., 2017) that binary mixtures of a MG and a FAME give simple, smooth
204 curves. These results imply that the solidification behaviors of MG/MG and MG/FAME
205 mixtures are different. We used the three thermodynamic models described in the previous
206 section to obtain theoretical liquidus curves and compared them with the experimental
207 curves.

208 The theoretical liquidus curves obtained with the non-solid-solution model are
209 shown by dashed-dotted lines in Figures 2 and 3. The model gives v-shaped curves; these

correspond to eutectic systems, which are widely found in lipid mixtures (Maximo et al., 2014). The theoretical curves obtained with the solid-solution model are shown by dashed lines. These monotonically increasing curves correspond to solid-solution systems, which are frequently found in binary systems composed of similar elements.

Figure 2 shows that the behavior of the α-type crystals depends on the pair of MGs. In the case of the MG12:0/MG18:0 mixture (Figure 2a), because of the difference between the carbon chain lengths (ΔC = 6), the experimental liquidus temperatures are close to those obtained with the non-solid-solution model. In contrast, the MG16:0/MG18:0 pair (Figure 2c; ΔC = 2) conforms to the solid-solution model. These results suggest that a large difference between the carbon chain lengths leads to independent solidification of the individual MGs, whereas similar MGs can form a solid solution. Such a tendency was reported by Maruyama et al. for binary systems of MGs (Maruyama et al, 1978). The behavior of the MG12:0/MG16:0 pair (Figure 2b; ΔC = 4) is intermediate between those indicated by the two models.

Figure 3 shows that for β-type crystals, the experimental liquidus curves are close to those obtained with the non-solid-solution model for all pairs, although there are some deviations. The reason for the difference between the behaviors of the α and β crystals remains unclear, but it could arise because of differences among the crystal transition rates of the MGs. In general, a MG with a shorter carbon chain has a shorter transition time

229 (Maruyama et al., 1971), therefore MGs with shorter chains will independently change to the
230 β form earlier than the those with longer chains and the solid solution will be disrupted
231 during the crystal transition.

232 The results obtained with the two models based on the solid–liquid equilibrium do
233 not fit the complex shapes of the liquidus curves well. The experimental curves have
234 irregularities, with multiple upward convex lines. We therefore used the compound formation
235 model, which is derived from the reaction equilibrium. The results obtained with this model
236 are shown by solid lines in Figures 2 and 3. These results clearly fit the experimental liquidus
237 curves well.

238 We will use Figure 3c, which is the simplest case, to explain the fitting procedure.
239 We first divided the experimental liquidus curve into three regions (I, II, and III). In regions I
240 and III, the compound formation model exactly matches the non-solid-solution model. This
241 means that only MG16:0 solidifies in region I ($\nu_1 = 1$, $\nu_2 = 0$) and only MG18:0 solidifies in
242 region III ($\nu_1 = 0$, $\nu_2 = 1$). On the basis of this assumption, the reaction equilibrium constant
243 $K_a$ for each region is $\gamma_1 x_1$ (region I) or $\gamma_2 x_2$ (region III), from equation (6). If the melting
244 point $T_{m,i}$ of the MG is chosen as the reference temperature $T_{ref}$, the compound formation
245 model, via equations (6) and (7), becomes identical to equation (3) for the non-solid-solution
246 model, i.e., the compound formation model includes the non-solid-solution model as a
247 special case.

248 The upward convex curve in region II is thought to indicate compound formation
249 between MG16:0 and MG18:0. For the calculation with equation (7), the highest temperature
250 in the given region was chosen as $T_{\mathrm{ref}}$. The stoichiometric numbers $\nu_1$ and $\nu_2$ were used as
251 fitting parameters and determined by the least-squares method. The $\Delta H_{\mathrm{ref}}$ term was estimated
252 as the average of the fusion enthalpies weighted by the stoichiometric numbers, as follows:

253 $$\Delta H_{\mathrm{ref}} = \frac{\nu_1 \Delta H_{m,1} + \nu_2 \Delta H_{m,2}}{\nu_1 + \nu_2} \quad (8)$$

254 When $\nu_1$ = 3.63 and $\nu_2$ = 2.25, the calculated curve fits the experimental plots well, as shown
255 in Figure 3c. For all cases in Figures 2 and 3, we counted the number of upward convex lines
256 to divide the curves into regions, and then fitting was performed independently for each
257 region in the same way. The obtained parameters are summarized in Table 2. Although we are
258 not certain whether or not the obtained stoichiometric numbers reflect the real world, it can
259 be said that the compound formation model can describe the complex solidification behaviors
260 of MGs.

261 Compound formation in MG mixtures is thought to occur because of the presence of
262 hydroxyl groups, which are involved in hydrogen bonding between MGs. Such strong
263 intermolecular interactions allow easy formation of associated molecules, which can be
264 distinguished by X-ray diffraction (Etter, 1990). Such compound-forming systems have also
265 been reported for triglyceride mixtures (Engström, 1992).

266

267 Multi-component mixtures

268 The compound formation model was applied to surrogate biodiesel fuels, namely
269 multi-component mixtures that consisted of MGs and FAMEs. A pair of MGs (1:1 by weight)
270 was added to a mixture of FAME12:0, FAME16:0, and FAME18:1 (65:24:11 by weight) at
271 various MG contents. The liquidus temperatures of the mixtures were determined by DSC,
272 via two methods; the results are shown in Figure 4 by open and solid circles, respectively. We
273 used MG contents higher than 2 wt% because at low contents the MG endothermic peaks in
274 the DSC curves were too weak. Although such high MG contents are rather far from those in
275 real biodiesel, we performed these experiments to investigate the potential of the model.

276 First, we determined the liquidus temperatures, which are shown by open circles in
277 Figure 4, by using the method described in the subsection of analytical method for α-type
278 MGs, in which the sample was immediately reheated after the first exothermic peak was
279 detected on cooling. However, sudden changes in the liquidus temperature can be observed,
280 especially in Figure 4a. This could be caused by the crystal transition from α to β′ or β,
281 because the transition time tends to become shorter in the presence of a solvent. FAMEs can
282 act as a solvent in this case, therefore the MGs sometimes change to the β′ or β type.
283 Determination of the liquidus temperature for α-type MGs in multi-component mixtures is
284 therefore difficult.

285 We therefore modified the DSC method and examined the sample after transition by

allowing an adequate transition time. For this purpose, the sample was cooled to −20 °C and then DSC was performed at a heating rate of 3 °C/min. The liquidus temperatures obtained by this method are shown as solid circles in Figure 4. In contrast to the previous results, the liquidus temperatures give monotonous curves. This method enabled us to obtain consistent liquidus curves for β′- or β-type MGs, although the crystal type was not specified in this study.

For calculations using the compound formation model, $T_{ref}$ was set at the highest liquidus point among the experimental data. Although the type of crystal was not identified, the enthalpies of fusion for the β type shown in Table 1 were used as tentative values for the calculation. The crystal type is not critical for testing the applicability of the model. The parameters $\nu_1$ and $\nu_2$ were determined by data fitting to be 0.00 and 1.19 for (a), 0.00 and 1.27 for (b), and 0.00 and 0.87 for (c), in Figure 4. The fitting results, which are represented by solid lines, show that the compound formation model works well for predicting the experimental liquidus curves. However, the values of $\nu_1$ and $\nu_2$ obtained by the model will not always reflect the actual stoichiometric numbers of the solid compounds, because these are just the results of data fittings.

The excellent matching of the compound formation model with the experimental data is not surprising because the model has fitting parameters. The compound formation model is therefore an empirical model. In a previous series of studies (Imahara et al., 2006;

305 Yoshidomi et al., 2017; Sugami et al., 2017), our ultimate purpose was to establish a
306 non-empirical formula for predicting the behaviors of any biodiesel and blends with fossil
307 diesel. The current study shows the complexity of MGs, even in the case of simple binary
308 mixtures. Although we successfully described the complex liquidus curves by using the
309 compound formation model, the parameters obtained will be useless for other cases because
310 the parameters will change if a different chemical component is used.

311 If the ratio of MGs is fixed, as in Figure 4, the compound formation model can be
312 used to predict biodiesel CFPs. This means that we can develop a formula for predicting the
313 CFPs of biodiesels derived from a feedstock as a function of the MG content by data fitting,
314 as in Figure 4, because the fatty acid composition is almost the same for a given type of
315 feedstock.

316

317 **Concluding remarks**

318 The liquidus temperatures of binary systems of MGs were determined by DSC to
319 investigate their interactions. Three thermodynamic models were applied to the obtained
320 results. The difference between the MG carbon chain lengths (ΔC) affected the liquidus curve
321 shape for α-type crystals. When ΔC was large (ΔC = 6), the liquidus curves were close to
322 those obtained with the non-solid-solution model, in which different MGs solidify
323 independently. When ΔC was small (ΔC = 2), the liquidus curve corresponded to the

solid-solution model, in which different MGs form a continuous solid solution.

These two models based on the solid–liquid equilibrium did not exactly fit the complicated liquidus curves of binary MGs. Only the compound formation model, which is derived from the reaction equilibrium, can describe the complicated behaviors of binary MGs. This implies that the different MGs form a solid compound via intermolecular hydrogen bonding. It was therefore concluded that the compound formation model is appropriate for describing the solidification behaviors of MGs.

The suitability of the compound formation model was tested for predicting the behaviors of surrogate diesel fuels that consisted of multi-component mixtures of MGs and FAMEs. The results show that the model represents the liquidus curves well. However, the compound formation model involves fitting parameters, which need to be determined from experimental data. The parameters will change depending on the chemical composition, therefore obtaining general predictions that apply to all cases is difficult. This model only works for biodiesel from known feedstocks. As a next step, we will apply this model to biodiesel fuels derived from various plant oils and establish a prediction formula for each feedstock.

**Conflict of interest**

The authors declare that they have no conflict of interest.

343

344 **References**

345 Chupka, G.M., Yanowitz, J., Chiu, G., Alleman T.L., & McCormick, R.L. (2011). Effect of
346 saturated monoglyceride polymorphism on low-temperature performance of biodiesel.
347 Energy Fuels, **25**:398–405.

348 Chupka, G.M., Fouts, L., Lennon, J.A., Alleman, T.L., Daniels, D.A., & McCormick, R.L.
349 (2014). Saturated monoglyceride effects on low-temperature performance of biodiesel
350 blends. Fuel Process Technol, **118**:302–309.

351 Committee for Standardization Automotive Fuels. (2008). Fatty acid methyl esters (FAME)
352 for biodiesel engines - Requirements and test methods (EN14214). Brussels: European
353 Committee for Standardization (CEN).

354 Coutinho, J.A.P., Gonçalves, M., Pratas, M.J., Batista, M.L.S., Fernandes, V.F.S., Pauly, J., &
355 Daridon, J.L. (2010). Measurement and modeling of biodiesel cold-flow properties.
356 Energy and Fuels, **24**:2667–2674.

357 Dunn, R.O., & Bagby, M.O. (1995). Low-temperature properties of triglyceride-based diesel
358 fuels: Transesterified methyl esters and petroleum middle distillate/ester blends. J Am
359 Oil Chem Soc, **72**:895–904.

360 Dunn, R. (2010). Cold Weather Properties and Performance of Biodiesel. In: The Biodiesel
361 Handbook, 2nd ed. Illinois: AOCS Press.

362 Engström, L. (1992). Triglyceride systems forming molecular compounds. Eur J Lipid Sci

363 Tech, **94**:173–181.

364 Etter, M.C. (1990). Encoding and decoding hydrogen-bond patterns of organic compounds.
365 Acc Chem Res, **23**:120–126.

366 Fischer, E., Bergmann, M., & Barwind, H. (1920). Neue synthese von a-monoglyceriden.
367 Berichte der Dtsch Chem Gesellschaft, 1589–1605. (in German)

368 Gmehling, J., Li, J., & Schiller, M. (1993). A modified UNIFAC model. 2. Present parameter
369 matrix and results for different thermodynamic properties. Ind Eng Chem Res, **32**:178–
370 193.

371 Imahara, H., Minami, E., & Saka, S. (2006). Thermodynamic study on cloud point of
372 biodiesel with its fatty acid composition. Fuel, **85**:1666–1670.

373 Knothe, G. (2005). Dependence of biodiesel fuel properties on the structure of fatty acid
374 alkyl esters. Fuel Process Technol, **86**:1059–1070.

375 Knothe, G., & Dunn, R.O. (2009). A comprehensive evaluation of the melting points of fatty
376 acids and esters determined by differential scanning calorimetry. J Am Oil Chem Soc,
377 **86**:843–856.

378 Lopes, J.C.A., Boros, L., Krähenbúhl, M.A., Meirelles, A.J.A, Daridon, J.L., Pauly, J.,
379 Marrucho, I.M., & Coutinho, J.A.P. (2008). Prediction of cloud points of biodiesel.
380 Energy and Fuels, **22**:747–752.

381 Lutton, E.S. (1971). The phases of saturated 1-monoglycerides C14-C22. J Am Oil Chem Soc,

382 **48**:778–781.

383 Lutton, E.S., & Jackson, F.L. (1967). Binary systems with monoglycerides. J Am Oil Chem
384 Soc, **44**:357–358.

385 Malkin, T., & Shurbagy, M.R.E. (1936). An x-ray and thermal examination of the glycerides.
386 Part II. The alpha-monoglycerides. J Chem Soc, 1628–1634.

387 Maruyama, T., Niiya, I., Imamura, M., Okada, M., Matsumoto, T., Horisawa, M., &
388 Matsumoto, T. (1971). Study on polymorphism of monoglyceride. I. Transition of crystal
389 modification of 1-monolaurin, 1-monomyristin, 1-monopalmitin, and 1-monostearin. J
390 Japan Oil Chem Soc, **20**:11–18. (in Japanese)

391 Maruyama, T., Niiya, I., Imamura, M., Okada, M., & Matsumoto, T. (1973). Study on
392 polymorphism of monoglyceride. II. Thermodynamic considerations on transition. J
393 Japan Oil Chem Soc, **22**:19–22. (in Japanese)

394 Maruyama, T., Niiya, I., Okada, M., & Matsumoto, T. (1979). Studies on polymorphism of
395 monoglycerides. VIII. Phase behavior of binary monoglycerides systems. J Japan Oil
396 Chem Soc, **28**:26–31. (in Japanese)

397 Maximo, G.J., Costa, M.C., Coutinho, J.A.P., & Meirelles, A.J.A. (2014). Trends and
398 demands in the solid–liquid equilibrium of lipidic mixtures. RSC Adv, **4**:31840–31850.

399 Sarin, A., Arora, R., Singh, N.P., Sarin, R., Malhotra, R.K., & Kundu, K. (2009). Effect of
400 blends of Palm-Jatropha-Pongamia biodiesels on cloud point and pour point. Energy,

401 **34**:2016–2021.

402 Smith, J.M., Van Ness, H.C., & Abbott, M.M. (2005). Introduction to chemical engineering
403 thermodynamics, 7th ed. New York: McGraw-Hill Education.

404 Sugami, Y., Yoshidomi, S., Minami, E., Shisa, N., Hayashi, H., & Saka, S. (2017). The effect
405 of monoglyceride polymorphism on cold-flow properties of biodiesel model fuel. J Am
406 Oil Chem Soc, **94**:1095–1100

407 Tang, H., Salley, S.O., & Ng, K.Y.S. (2008). Fuel properties and precipitate formation at low
408 temperature in soy-, cottonseed-, and poultry fat-based biodiesel blends. Fuel, **87**:3006–
409 3017.

410 Tumakaka, F., Prikhodko, I.V., & Sadowski, G. (2007). Modeling of solid–liquid equilibria
411 for systems with solid-complex phase formation. Fluid Phase Equilib, **260**:98–104.

412 Yoshidomi, S., Sugami, Y., Minami, E., Shisa, N., Hayashi, H., & Saka, S. (2017). Predicting
413 solid–liquid equilibrium of fatty acid methyl ester and monoacylglycerol mixtures as
414 biodiesel model fuels. J Am Oil Chem Soc, **94**:1087–1094.

415

**List of Tables**

**List of Figures**

**Table 1** Thermodynamic properties of monoglycerides

| Component and type of crystal | | Melting point, °C | Enthalpy of fusion, kJ/mol | Number of UNIFAC functional group | | | | | |
|---|---|---|---|---|---|---|---|---|---|
| | | | | $CH_3$ | $CH_2$ | CH | OH(p) | OH(s) | $CH_2COO$ |
| MG12:0 | α | 44.4 | 22.4 | 1 | 11 | 1 | 1 | 1 | 1 |
| (1-monolaurin) | β | 62.1 | 47.5 | | | | | | |
| MG16:0 | α | 64.9 | 34.4 | 1 | 15 | 1 | 1 | 1 | 1 |
| (1-monopalmitin) | β | 72.8 | 67.1 | | | | | | |
| MG18:0 | α | 71.6 | 35.1 | 1 | 12 | 1 | 1 | 1 | 1 |
| (1-monostearin) | β | 78.9 | 75.2 | | | | | | |

**Table 2** Parameters obtained by using compound formation model for various binary mixtures of MGs and crystalline forms

| Number of regions | Parameters | $C_1$ = MG12:0 $C_2$ = MG18:0 | | $C_1$ = MG12:0 $C_2$ = MG16:0 | | $C_1$ = MG16:0 $C_2$ = MG18:0 | |
|---|---|---|---|---|---|---|---|
| | | α | β | α | β | α | β |
| 1 | $T_{ref}$, °C | 44.4 | 62.1 | 44.4 | 62.1 | 64.9 | 72.8 |
| | $v_1$ | 1.00 | 1.00 | 1.00 | 1.00 | 1.00 | 1.00 |
| | $v_2$ | 0.00 | 0.00 | 0.00 | 0.00 | 0.00 | 0.00 |
| 2 | $T_{ref}$, °C | 46.6 | 62.9 | 43.9 | 60.7 | 66.8 | 72.4 |
| | $v_1$ | 0.79 | 2.11 | 0.002 | 0.18 | 0.74 | 3.63 |
| | $v_2$ | 0.50 | 1.12 | 0.07 | 0.32 | 0.07 | 2.25 |
| 3 | $T_{ref}$, °C | 57.4 | 73.7 | 47.2 | 64.2 | 67.5 | 78.9 |
| | $v_1$ | 0.65 | 0.10 | 1.19 | 0.44 | 0.23 | 0.00 |
| | $v_2$ | 1.22 | 2.24 | 0.81 | 1.11 | 0.21 | 1.00 |
| 4 | $T_{ref}$, °C | 70.6 | 71.6 | 54.4 | 71.7 | 70.9 | - |
| | $v_1$ | 0.18 | 0.00 | 1.44 | 0.20 | 0.09 | - |
| | $v_2$ | 1.37 | 1.00 | 2.39 | 3.17 | 0.57 | - |
| 5 | $T_{ref}$, °C | 71.6 | - | 64.9 | 72.8 | 71.6 | - |
| | $v_1$ | 0.00 | - | 0.00 | 0.00 | 0.00 | - |
| | $v_2$ | 1.00 | - | 1.00 | 1.00 | 1.00 | - |

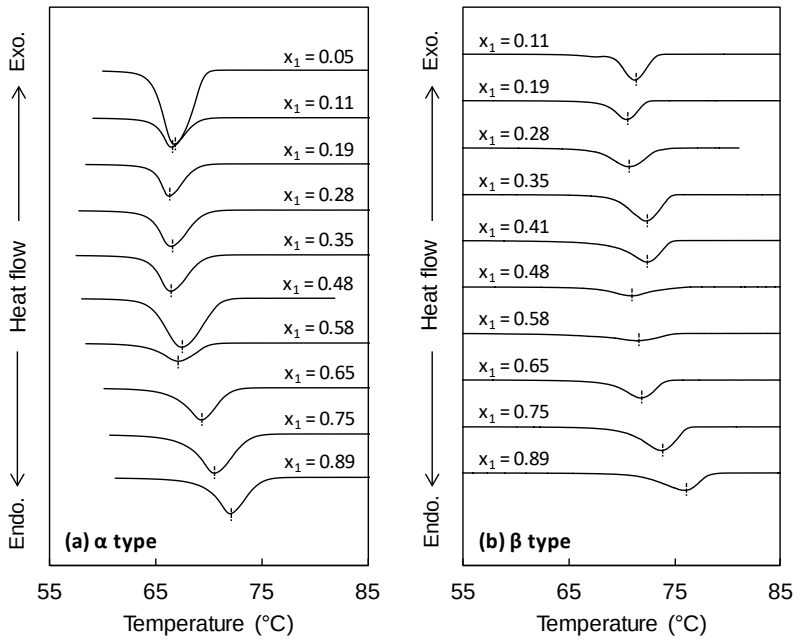
Exo.
Heat flow
Endo.
x1 = 0.05
x1 = 0.11
x1 = 0.19
x1 = 0.28
x1 = 0.35
x1 = 0.48
x1 = 0.58
x1 = 0.65
x1 = 0.75
x1 = 0.89
(a) α type
55
65
75
85
Temperature (°C)
Exo.
Heat flow
Endo.
x1 = 0.11
x1 = 0.19
x1 = 0.28
x1 = 0.35
x1 = 0.41
x1 = 0.48
x1 = 0.58
x1 = 0.65
x1 = 0.75
x1 = 0.89
(b) β type
55
65
75
85
Temperature (°C)

**Fig. 1**

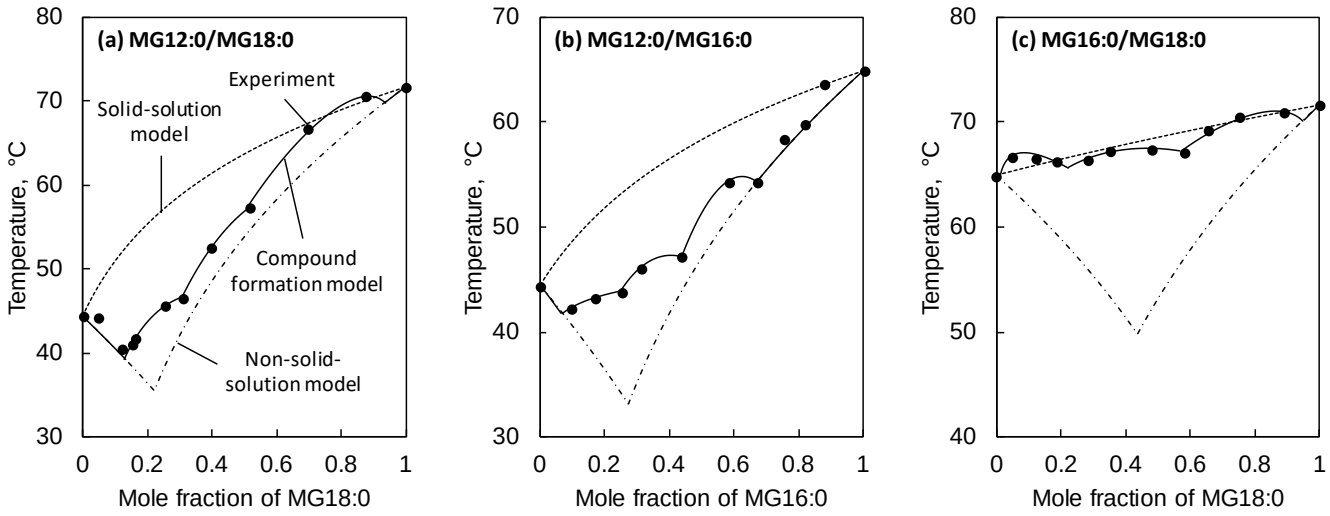
(a) MG12:0/MG18:0
Experiment
Solid-solution model
Compound formation model
Non-solid-solution model
Temperature, °C
Mole fraction of MG18:0
(b) MG12:0/MG16:0
Temperature, °C
Mole fraction of MG16:0
(c) MG16:0/MG18:0
Temperature, °C
Mole fraction of MG18:0

**Fig. 2**

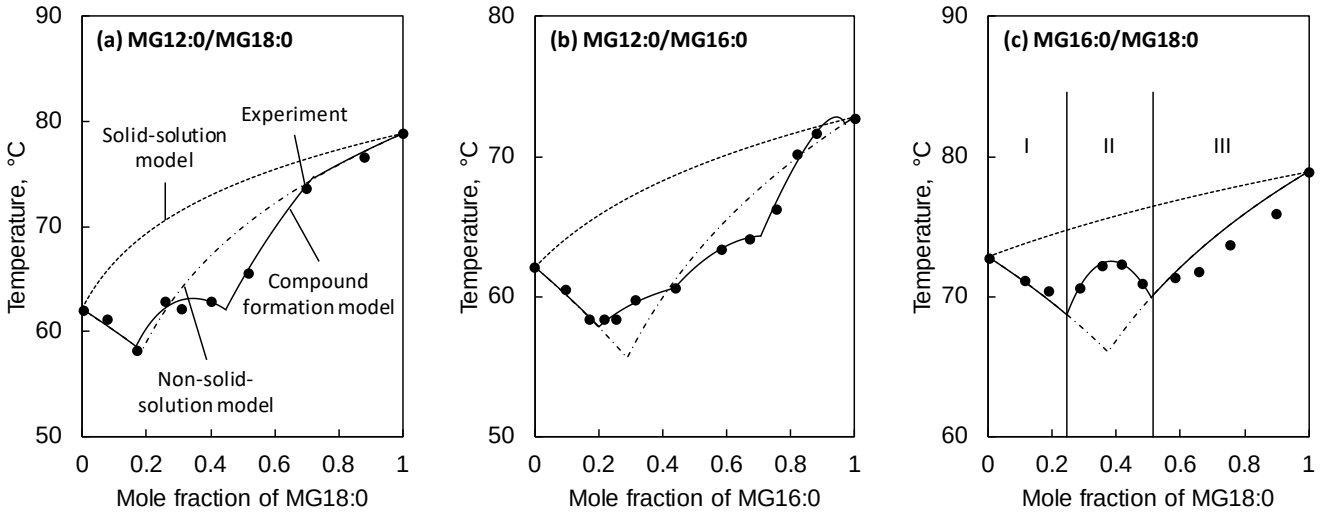
(a) MG12:0/MG18:0
Solid-solution model
Experiment
Compound formation model
Non-solid-solution model
Temperature, °C
Mole fraction of MG18:0
(b) MG12:0/MG16:0
Temperature, °C
Mole fraction of MG16:0
(c) MG16:0/MG18:0
I
II
III
Temperature, °C
Mole fraction of MG18:0

**Fig. 3**

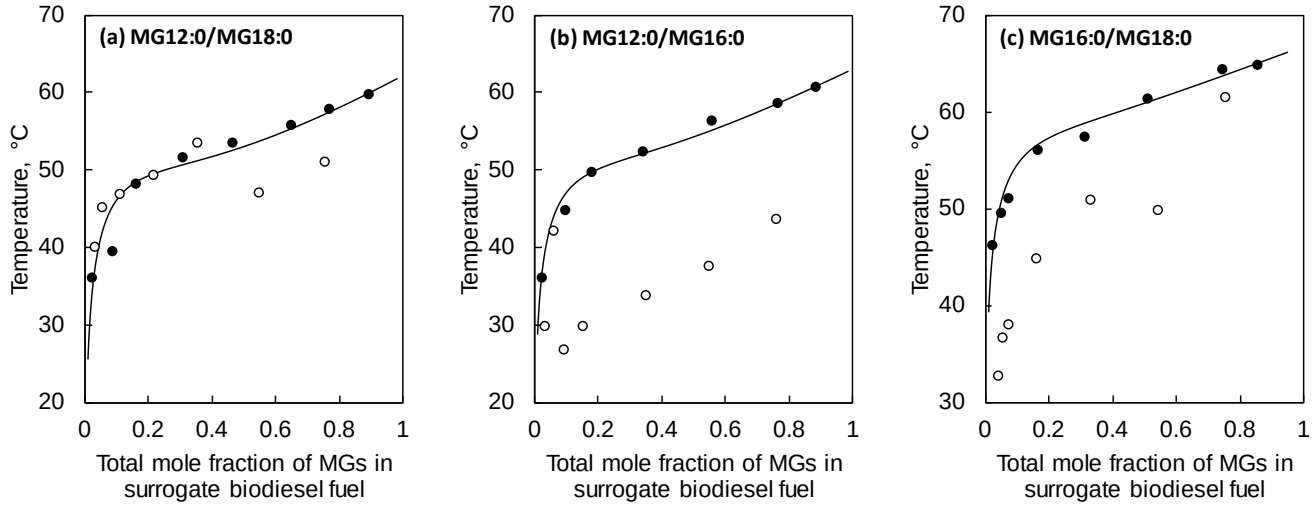
(a) MG12:0/MG18:0
(b) MG12:0/MG16:0
(c) MG16:0/MG18:0
Temperature, °C
Total mole fraction of MGs in surrogate biodiesel fuel

**Fig. 4**